

Crystalline fluidized beds

M.A. Rutgers,^{1,*} J.-Z. Xue,^{1,2} E. Herbolzheimer,² W.B. Russel,³ and P.M. Chaikin^{1,2}¹*Department of Physics, Princeton University, Princeton, New Jersey 08540*²*Exxon Research and Engineering Company, Route 22 East, Annandale, New Jersey 08801*³*Department of Chemical Engineering, Princeton University, Princeton, New Jersey 08540*

(Received 21 September 1994)

By using a solvent counterflow (i.e., fluidization) to prevent sedimentation of charged silica spheres, we have established a steady state polycrystalline colloidal suspension of uniform concentration. With this technique we varied the steady state concentration of a single sample by simply changing the flow rate. Bragg scattering from the fluidized bed allowed for direct investigation of its crystal structure, stability, uniformity, and volume fraction, while the interparticle interactions were directly measured from shear resonances of the bulk. For strongly repulsive interactions we found that the particles formed an fcc lattice and sedimented considerably more slowly than when in a highly disordered state.

PACS number(s): 82.70.Dd, 47.55.Kf, 47.15.Gf

Sedimentation and fluidization have been widely studied for close to a century since they are important in understanding and predicting natural and technological processes ranging from the silting of rivers and the formation of sedimentary rocks to the design of chemical reactors and waste treatment plants to the formation and subsequent properties of materials such as ceramics. Sedimentation rates are also a primary test of our knowledge of the hydrodynamic interactions between particles in suspension [1–4]. Nevertheless, understanding the impact of particle dynamics on the microscale structure, and hence on the average sedimentation rate, remains a challenging problem for even the simplest case of uniformly sized spheres at low Reynolds number. To date, exact solutions exist only for the one- and two-body problems or for particles positioned in a periodic array. For a face centered cubic (fcc) array [5], for example, the normalized sedimentation velocity $K(\phi) \equiv v(\phi)/v_{\text{Stokes}}$ is given by $1 - 1.791\phi^{1/3} + \dots$, where ϕ is the particle volume fraction, $v_{\text{Stokes}} = \frac{2}{9}a^2(\rho_p - \rho_{\text{liq}})g/\eta$ is the terminal velocity of an isolated sphere, g is the gravitational constant, a is the radius of the particle, ρ_p is its density, and ρ_{liq} and η are, respectively, the density and viscosity of the suspending fluid. These calculations can be extended to cover the entire range of concentrations for any type of lattice [1,2]. The usefulness of these results has been unclear, however, because the periodic structure is known to be hydrodynamically unstable. For instance, when fluctuations bring two particles on a hypothetical lattice closer than the average separation, they sediment faster than the average and destabilize the lattice, leading quickly to disorder.

The other extreme is a random suspension for which a primary theoretical challenge is the fact that summing the hydrodynamic interactions, which decay inversely with particle separation, over a large number of

particles leads to divergent integrals. Batchelor showed how to overcome this difficulty and found that $K(\phi) = 1 - 6.55\phi + O(\phi^2)$ for a dilute random suspension [6]. There have been several efforts to extend these calculations to higher concentrations [4,7–10], but a second problem arises in that the settling of particles also determines the microscale structure through a complex set of hydrodynamic and nonhydrodynamic interactions. This structure can in turn strongly influence the average settling velocity and particle dynamics.

In this paper we present measurements on the settling velocity of spheres at low Reynolds number while simultaneously controlling and measuring the suspension microstructure. The particles used were charged spheres of 3-methacryloxypropyltrimethoxysilane stabilized silica, 0.6 μm in diameter, suspended in a refractive index matched fluid mixture of ethanol and toluene [11]. The density mismatch of 1.0 g/cm^3 between the liquid and the silica resulted in a sedimentation velocity of at most several micrometers per minute. This system had sufficiently strong repulsive interactions that the spheres formed fcc crystals which were stable against thermal and hydrodynamic fluctuations for volume fractions down to 0.2. By adding counterions we were able to decrease the strength of the repulsions so that the crystal melted. Hence we could measure directly the effects of the microstructure on the sedimentation velocity.

As shown in Fig. 1, we collected our measurements from a fluidized bed rather than from batch settling experiments as is more commonly done. The advantages of fluidization include the following: (1) the suspension is indefinitely stable and uniform; (2) steady state can be achieved and observed well after initial transients have decayed; (3) the true sedimentation velocity can be measured (by the required counterflow) without questions of spreading or instability of the upper sedimentation front; (4) the volume fraction can be continuously controlled by changing the flow rate; and (5) the particle interactions, and thereby the suspension microstructure, can be altered with ions carried into the bed by the fluid. To see

* Author to whom correspondence should be addressed.

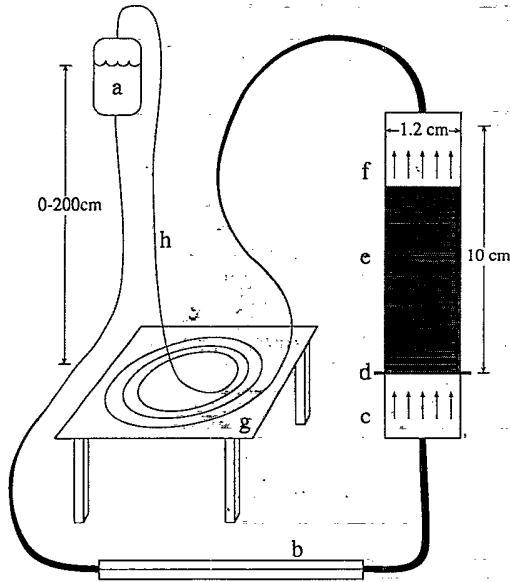


FIG. 1. Experimental setup: (a) a fluid reservoir supplies a pressure drop across (b) a glass capillary. The reservoir's height controls the pressure and thereby the flow rate. (c) The fluidized bed consists of a rectangular glass tube ($1.2 \times 0.2 \times 10 \text{ cm}^3$) with (d) an alumina membrane, permeable to fluid only, at the bottom. The liquid flows through (e) the colloidal suspension and (f) out of the cell where it accumulates in (g) a long thin tube. The flow rate, measured from the rate at which the tube fills, is typically less than 1 cm^3 every 10 days.

how these advantages arise, consider the distribution of particle concentration which is governed by the expression for the flux of particles in the vertical (x) direction, given by

$$\phi v_p = \phi v_s + \phi \frac{K(\phi) V_p}{6\pi\eta a} \left(-\Delta\rho g - \frac{1}{\phi} \frac{\partial \Pi}{\partial x} \right) - D_H \frac{\partial \phi}{\partial x}, \quad (1)$$

where v_p is the velocity of the particles, V_p is the particle volume, v_s is the average superficial velocity of the supporting fluid (defined as the volumetric flow of solvent entering the column divided by the column's cross sectional area), $\Delta\rho$ is the density difference between the particles and the solvent, Π is the osmotic pressure acting on the particles, $1/K(\phi)$ is the increased Stokes drag due to hydrodynamic interactions, and D_H is the hydrodynamic dispersion coefficient. The terms on the right-hand side show that the particles (i) translate with the average suspension velocity; (ii) and (iii) slip relative to this motion due to forces applied by, respectively, gravity and gradients in osmotic pressure (e.g., thermal motions and Coulombic repulsion of the particles); and (iv) "diffuse" down a concentration gradient due to hydrodynamic dispersion. This last term is relatively small for our system since thermal fluctuations are much larger than hydrodynamic fluctuations. We will show later that their relative importance depends on the Péclet number $Pe = vl/D$, where v is the particle velocity, l is a relevant length scale, and D is the Stokes-Einstein diffusion constant. If

we take $l = 2a$ and $v = v_{\text{Stokes}}$ we get a maximum value for the Péclet number of $Pe = 2(\frac{4}{3}\pi a^4 \Delta\rho g / k_B T) \approx 0.16$, which implies that thermal fluctuations will dominate.

Let us consider briefly some limiting cases of Eq. (1). In equilibrium, with no sedimentation or counterflow, the density profile is set by the osmotic pressure gradient. At low volume fractions $\Pi = nk_B T = \phi k_B T / V_p$, as for an ideal gas, where n is the particle number density, k_B the Boltzmann constant, T the temperature, and V_p the particle volume. For this low volume fraction limit of a nonfluidized sediment, Eq. (1) gives a density profile of the same form as the exponential law of atmospheres $\phi_{\text{lim}\phi_0 \rightarrow 0} = \phi_0 e^{-z/h}$ with a gravitational height $h \equiv 3k_B T / 4\pi a^3 \Delta\rho g$ and a maximum density ϕ_0 at the bottom of the sediment. For our system, $h \approx 3.7 \mu\text{m}$ or about six particle diameters. On the other hand, if we neglect the osmotic pressure term and impose no solvent counterflow we have $\frac{4}{3}\pi a^3 \Delta\rho g = -6\pi\eta a v_p / K(\phi)$, which illustrates that $K(\phi) = v_p / v_{\text{Stokes}}$ is the normalized sedimentation velocity for a hydrodynamically interacting system with volume fraction ϕ . Finally, if we impose a counterflow v_s , the steady state profile will consist of a region of near constant ϕ determined by $v_{\text{Stokes}} K(\phi) = v_s$ and a transition region in which ϕ drops from ϕ_{bulk} to 0 over a height $\sim O(h)$.

We obtained the desired colloidal crystals after several weeks of fluidization. Crystals typically grew from the bottom up, as the initially dilute suspension settled to its steady state fluidized condition. The crystalline region is easily discernible by its randomly oriented crystallites, typically a few tenths of a millimeter on a side, which Bragg scatter white light at particular wavelengths (for a given illumination angle) and have a brilliant opalescent appearance. For $\phi > 0.3$ the crystallites do not flow or change orientation for at least a month, provided there are no significant perturbations in the flow rate of the liquid entering the column. We let the fluidized crystals relax to steady state at various fluidization rates. Bragg scattered light from a collimated laser beam allowed us to measure the fcc crystal structure and lattice spacing, while scanning the beam through the bulk of the crystal confirmed its uniform density. The volume fraction was calculated from the crystal structure, lattice spacing, and particle size. The results for the dependence of the sedimentation velocity on volume fraction for the fcc structure are shown in Fig. 2, in addition to numerical simulation results [4] and some experimental observations [12,3] for hard sphere sedimentation, as well as the theoretical predictions for spheres in an fcc array [$K_{\text{fcc}}(\phi)$] [1,2]. Our data lie slightly above the $K_{\text{fcc}}(\phi)$ calculations, which may suggest that these crystals are sufficiently "weak" that the thermal motion of the particles about their equilibrium positions leads to a sedimentation velocity between those of perfectly ordered and randomly disordered arrays.

The sample's polycrystallinity could also contribute to this small discrepancy either through the crystallite orientations or through the disorder introduced by the grain boundaries. The former has no effect because the viscous drag on the cubic arrays is independent of their orientation with respect to the flow, as can easily be proven

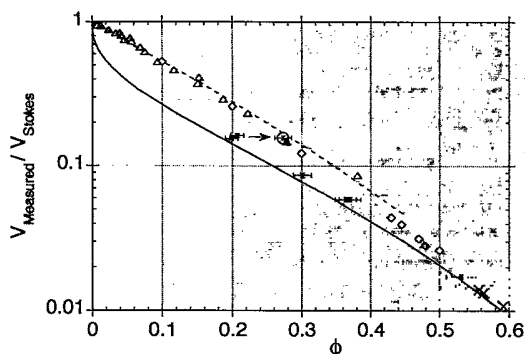


FIG. 2. Volume fraction dependence of the normalized sedimentation velocity. — —, a particular simulation by Ladd [4] for disordered hard spheres and measurements (\diamond , Δ) by Paulin and Ackerson [12] and Buscall *et al.* [3], respectively; —, smooth fit to exact calculations of Zick and Homay [1] for an fcc lattice; \times , a measurement of randomly stacked hard sphere crystals by Paulin and Ackerson [12]; \bullet , our measurement of a polycrystalline fcc colloidal crystal; \circ , the steady state disordered fluidized bed after the addition of screening ions.

from the linearity of the Stokes equations which govern the fluid motion. At the grain boundaries there should be a loss of long range positional order but no significant change in particle density, because the repulsive interparticle potential will keep the sphere separations similar to those in the crystal. Hence the fluid permeability of the boundaries should be similar to that of the crystal.

We verified this by taking advantage of our fluidization technique to make deliberate microstructural changes to the suspension. At first we destroyed only the long range order, leaving short range order intact, by simply expanding the bed beyond $\phi \approx 0.2$ where the crystallites were observed to melt. At this time Bragg reflections disappeared, but the structure function retained a distinct maximum, indicating that the fluid had strong local order and a well defined nearest neighbor distance. This state is a bulk manifestation of the grain boundaries described earlier. We then incrementally decreased the flow rate until crystallization was again observed, during which the bed height increased by about $2\% \pm 1\%$, translating into a decrease in volume fraction of only 0.01. The fact that the sedimentation rate changes so little through the phase transition implies that the particles at the grain boundaries experience essentially the same drag as those in the crystallites.

A more dramatic effect was induced when we suppressed the electrostatic repulsion between particles, which triggered much larger changes in the microstructure. We took a uniform, crystalline sample at $\phi = 0.2$ and left the flow rate unchanged while we "turned off" the interparticle repulsions by adding sufficient HCl to the fluid supply reservoir to essentially screen out the electrostatic interactions between the particles. When the new solution (3 mM HCl) flowed through the crystal the opalescence disappeared immediately, indicating a loss of long and short range order, and during the next few weeks of settling the sample height decreased linearly with time until it stabilized at 22% below the original

height (Fig. 3). As shown in Fig. 2, the higher volume fraction of $\phi = 0.28$ for the same sedimentation rate is in quantitative agreement with $K_{\text{disordered}}(\phi)$ for hard spheres. Purging the salt from the system caused the bed to return to its initial crystalline condition.

From the combination of these two tests we made some conclusions that may cast light on the mechanism that most strongly influences the sedimentation velocity. The three different states explored in our experiment gave increasing freedom of motion to the particles. The change from crystal to ordered fluid introduced the possibility of relative particle motion, but had no measurable effect on the sedimentation velocity. The change from repulsive spheres to nearly hard spheres increased the probability of fluctuations in the particle number density. More concentrated regions settle faster than their surroundings and this tends to increase the average sedimentation velocity. A typical example [6] would be a pair of nearly touching particles which sediments faster than a relatively isolated sphere. A system with strongly repulsive interactions, on the other hand, maximizes interparticle separations which in turn inhibits density fluctuations that could lead to an increased sedimentation rate.

Further support for the source of the changes in the sedimentation velocity and microstructure was obtained by determining the strength of the interparticle potential by measuring the elastic shear modulus of the colloidal crystal [13]. Standing shear waves inside the polycrystalline sample were excited by laterally tapping the flow cell and the frequency of these modes was observed by detecting the oscillations of the Bragg peaks using a position sensitive photodiode and a lock-in amplifier. The shear modulus increased from 3 to 100 dyn/cm² as the

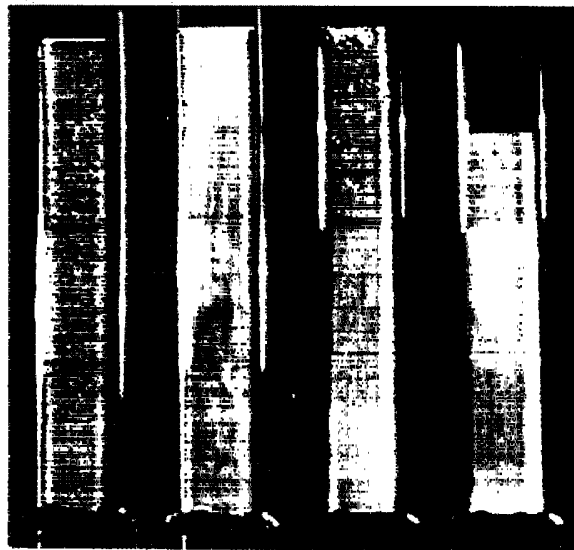


FIG. 3. Shown from left to right are a stable uniform crystalline fluidized bed at 0.2 volume fraction (slight height suppression due to a temperature change), a dilute acid infusion (10 μM) reduces crystallite size, but leaves the height unchanged, a partially melted crystal due to a more heavily screening ion infusion (3 mM), and a few weeks later, the final stable disordered state at 0.28 volume fraction.

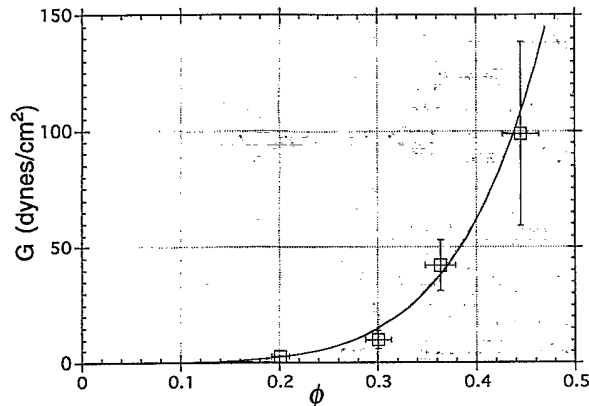


FIG. 4. Shear modulus of the fluidized colloidal crystal as a function of volume fraction. \square , measurement of the shear modulus; —, fit from a simple model by Buscall *et al.* [14] with a 11.5-mV surface potential and a 1 μ M electrolyte concentration.

volume fraction was increased from 0.2 to 0.45 (Fig. 4.) With reasonable agreement the data fit a simple model for the shear modulus, developed by Buscall *et al.* [14], which assumes nearest neighbor screened Coulomb interactions. From this fit we estimated a particle surface potential of $\Psi_s = 12$ mV.

Using the measured modulus we can check whether the interparticle forces are indeed sufficiently strong to stabilize the crystal against thermal and hydrodynamic fluctuations. In a simple model the phenomenological Lindemann [15] criterion states that a solid melts when the rms deviation of a particle from its lattice site exceeds a certain fraction α of the distance to a near neighbor r_{NN} , $\langle \delta r^2 \rangle / r_{NN}^2 \approx \alpha^2 \approx 0.04$. In a simple model, the particle is harmonically bound to its lattice site with a force constant which is an elastic modulus times a nearest neighbor distance $F = G \times r_{NN} \delta r$. For thermal fluctuations, $\langle (\delta r)^2 \rangle$ can be estimated from the equipartition theorem and the shear modulus G : $G r_{NN} \langle (\delta r)^2 \rangle / 2 \approx k_B T / 2$. Combined with the Lindemann criterion this dictates a minimum value for the elastic constant: $G_T > k_B T / r_{NN}^3 \alpha^2 \approx 25 n k_B T$. Since $G(n)/n$ is monotonic with n , we expect that the crystal should melt at small n . Indeed, in our experiment we find that the crystals melt below $\phi = 0.2$ where the shear modulus of the crystal was measured as $G \approx 30 n k_B T$. The crystal must also be sufficiently strong to resist hydrodynamic fluctuations. The random displacements caused by the particle velocity variance can be estimated from the Stokes drag, $G r_{NN} \delta r_{rms} = \delta V_{rms} 6 \pi \eta a$. For sedimentation the variance in the settling velocity scales with the average sedimentation rate and depends on ϕ , $\sqrt{\langle \delta V^2 \rangle} = v_{Stokes} W(\phi)$. Combined with the Lindemann criterion, the definition of the Péclet number, and the renormalization by $K(\phi)$ we find that the minimum elastic constant to resist hydrodynamic melting (G_H) relative to that required to resist thermal melting (G_T) is $G_H/G_T = (Pe r_{NN}/a)[W(\phi)/K(\phi)]$. The value of the Péclet number dominates this expression since both r_{NN}/a and $W(\phi)/K(\phi)$ are order one [16] at the relatively

high volume fractions of this experiment. Since we are at relatively low Péclet number, thermal fluctuations dominate and our main concern is thermal stability, which is satisfied. Interestingly, although the shear modulus is sufficiently strong to combat both hydrodynamic and thermal fluctuations, it is only strong enough to support about 5 monolayers of particles; hence the fluidization is essential to prevent the collapse of the bed.

Finally, given the surface potential we calculated from the shear modulus measurements, we can also confirm that electroviscous effects arising from the double layer surrounding the particles do not significantly affect their sedimentation velocity. In the limit of thin double layers, Smulochowski [17] calculated the fractional correction in the sedimentation velocity of an isolated sphere as $v/v_{Stokes} = 1 - (\epsilon^2 \Psi_s^2 / 16 \pi^2 a^2 \lambda \eta)$, where ϵ and λ are, respectively, the liquid dielectric constant and conductivity and ψ is the particle surface potential. Corrections to this prediction, which account for thicker double layers and for particle interactions in dilute suspensions, have also been calculated [18,19]. For our system we estimated a dimensionless surface potential $e \Psi_s / k_B T = 0.45$, where e is the electronic charge, and a normalized Debye screening length $\kappa a = 4$ corresponding to a liquid conductivity of $\lambda \approx 5 \times 10^{-7} \Omega^{-1}/\text{cm}$. For low concentrations this predicts a correction to the sedimentation velocity of no more than 0.01% and hence the changes in sedimentation velocity we measured above are not due to electroviscous effects.

Our development of a colloidal fluidized bed has proven fruitful for measuring several aspects of the relationship between suspension microstructure and sedimentation velocity. An important accomplishment has been the experimental verification of the calculated settling velocity of an fcc crystal, for volume fractions down to 0.2. The bed has offered unprecedented control over suspension volume fraction and solvent properties, both of which were used to induce changes in the microstructure. We have also shown the technique useful for growing colloidal crystals in a system which otherwise cannot support its own weight and it simultaneously gave an opportunity to measure the crystal's mechanical properties. The use of a fluidized bed to study interacting particles has many advantages that await further exploitation. At lower ϕ we should be able to see the unusual $\phi^{1/3}$ dependence of the sedimentation velocity. At higher sedimentation rates we should see hydrodynamic melting rather than thermal melting. By systematically altering the salt concentration we can better study the suppression of the velocity variance [16] due to particle repulsions. Inverting the flow in a much more strongly interacting system provides an easy way of studying the osmotic pressure vs ϕ . Finally, we have found the technique useful for purifying a bidisperse particle suspension.

We thank N.J. Wagner for synthesizing the sample. We also thank M.O. Robbins, D.J. Pine, J.F. Brady, D.A. Saville, and again N.A. Wagner for useful discussions during the course of this experiment. This work was partially supported under NASA Contract No. NAG3-1158.

- [1] A. A. Zick and G. M. Homsy, *J. Fluid Mech.* **115**, 13 (1982).
- [2] A. S. Sangani and A. Acrivos, *Int. J. Multiphase Flow* **8**, 343 (1982).
- [3] R. Buscall, J. W. Goodwin, R. H. Ottewill, and T. F. Tadros, *J. Colloid Interface Sci.* **85**, 78 (1982).
- [4] A. J. C. Ladd, *J. Chem. Phys.* **93**, 3484 (1990).
- [5] H. Hasimoto, *J. Fluid Mech.* **5**, 317 (1959).
- [6] G. K. Batchelor, *J. Fluid Mech.* **52**, 245 (1972).
- [7] C. W. J. Beenakker and P. Mazur, *Physica A* **120**, 388 (1983).
- [8] C. W. J. Beenakker and P. Mazur, *Physica A* **126**, 349 (1984).
- [9] J. F. Brady and L. J. Durlofsky, *Phys. Fluids* **31**, 717 (1988).
- [10] A. J. C. Ladd, *Phys. Fluids A* **5**, 299 (1992).
- [11] A. P. Philipse and P. Vrij, *J. Colloid Interface Sci.* **128**, 121 (1989).
- [12] S. Paulin and B. J. Ackerson, *Phys. Rev. Lett.* **64**, 2663 (1990).
- [13] P. Pieranski, *Contemp. Phys.* **24**, 25 (1983).
- [14] R. Buscall, J. W. Goodwin, M. W. Hawkins, and R. H. Ottewill, *J. Chem. Soc. Faraday Trans.* **78**, 2873 (1982).
- [15] F. A. Lindemann, *Z. Phys.* **11**, 609 (1910).
- [16] J. Z. Xue *et al.*, *Phys. Rev. Lett.* **69**, 1715 (1992).
- [17] M. V. Smulochowski, *Graetz Handbuch der Elektrizitaet und des Magnetismus, Vol. II* (T.A. Barth, Leipzig, 1921).
- [18] D. A. Saville, *Adv. Colloid Interface Sci.* **16**, 267 (1982).
- [19] H. Ohshima, T. W. Healy, L. R. White, and R. W. O'Brien, *J. Chem. Soc. Faraday Trans.* **2 80**, 1299 (1984).